Role of salt bridges in the dimer interface of 14-3-3ζ in dimer dynamics, N-terminal α-helical order, and molecular chaperone activity

Received for publication, June 7, 2017, and in revised form, October 24, 2017 Published, Papers in Press, November 6, 2017, DOI 10.1074/jbc.M117.801019

Joanna M. Woodcock[‡1,2], Katy L. Goodwin[§1], Jarrod J. Sandow[¶‖1], Carl Coolen[‡], Matthew A. Perugini[**], Andrew I. Webb[¶‖], Stuart M. Pitson[‡3,4], Angel F. Lopez[‡3], and John A. Carver[‡‡3]

From the [‡]Centre for Cancer Biology, University of South Australia and SA Pathology, Adelaide, South Australia 5000, the [§]School of Physical Sciences, University of Adelaide, Adelaide, South Australia 5005, the [¶]Division of Systems Biology and Personalised Medicine, Walter and Eliza Hall Institute of Medical Research, Parkville, Victoria 3052, the [‖]Department of Medical Biology, University of Melbourne, Parkville, Victoria 3052, the [**]Department of Biochemistry and Genetics, La Trobe Institute for Molecular Science, La Trobe University, Melbourne, Victoria 3086, and the [‡‡]Research School of Chemistry, Australian National University, Acton, Australian Capital Territory 2601, Australia

Edited by Wolfgang Peti

The 14-3-3 family of intracellular proteins are dimeric, multifunctional adaptor proteins that bind to and regulate the activities of many important signaling proteins. The subunits within 14-3-3 dimers are predicted to be stabilized by salt bridges that are largely conserved across the 14-3-3 protein family and allow the different isoforms to form heterodimers. Here, we have examined the contributions of conserved salt-bridging residues in stabilizing the dimeric state of 14-3-3ζ. Using analytical ultracentrifugation, our results revealed that Asp[21] and Glu[89] both play key roles in dimer dynamics and contribute to dimer stability. Furthermore, hydrogen-deuterium exchange coupled with mass spectrometry showed that mutation of Asp[21] promoted disorder in the N-terminal helices of 14-3-3ζ, suggesting that this residue plays an important role in maintaining structure across the dimer interface. Intriguingly, a D21N 14-3-3ζ mutant exhibited enhanced molecular chaperone ability that prevented amorphous protein aggregation, suggesting a potential role for N-terminal disorder in 14-3-3ζ's poorly understood chaperone action. Taken together, these results imply that disorder in the N-terminal helices of 14-3-3ζ is a consequence of the dimer–monomer dynamics and may play a role in conferring chaperone function to 14-3-3ζ protein.

The family of 14-3-3 proteins are important regulators of signaling responses in eukaryotic cells. They are dimeric phosphoserine-binding proteins that, via binding to dual phosphoserine motifs in target proteins, undertake many roles from sequestration of proteins away from alternative interactions to conformationally altering proteins to bring about functional changes in their activity (1, 2). For example, the sequestration of phospho-forms of Cdc25 phosphatase, FoxO transcription factors, and the BH3 protein BAD by 14-3-3 proteins from their sites of function attenuates the activities of these proteins (1, 2). Through conformational restraint, 14-3-3 proteins also regulate many enzymatic activities, such as the serine kinases Raf-1 and apoptosis signal-regulating kinase-1 (1, 2). Less well understood is the ability of 14-3-3 proteins to act as molecular chaperones, preventing the aggregation of unfolding proteins under conditions of cellular stress, such as elevated temperature (3). The chaperone action of 14-3-3ζ is not phosphorylation-dependent and occurs by mechanisms distinct from 14-3-3's phospho-binding functions (4).

The mammalian 14-3-3 protein family comprises seven isoforms (β, ε, γ, η, τ, σ, and ζ), which are encoded by separate genes but exhibit a high degree of sequence and hence structural similarity (5). The crystal structures of all seven 14-3-3 isoforms in homodimeric form have been determined and show that they all exhibit the same overall structure (5). Each monomer is composed of nine α-helices arranged in a curved palisade that forms a distinct cup shape that represents the phosphoserine peptide-binding groove (5). Each monomer also has a short flexible region at the extreme C terminus (4), which plays a role in regulating the access of phosphoserine clients to the binding groove (6). The monomer subunits form dimers via their N-terminal helices with salt bridges between the first two helices of one monomer (αA and αB) and the fourth helix of the other monomer (αD) predicted to hold the dimers together (5). The postulated salt bridges include Arg[18]-Glu[89] (ζ numbering used here, conserved in all isoforms), Asp[21]-Lys[85] (conserved in all except ε in which the Asp[21] equivalent is Glu[22] and Lys[85] is Met[88]), and Glu[5]-Lys[74] (conserved with the exception of η, γ, ε, and σ) (5). Other more transient salt bridges have also been identified in 14-3-3ζ between Lys[9]-Glu[81] or the N-terminal α-amino group and Glu[81] (7), although these residues are not conserved in all isoforms (Lys[9] is absent in ε, and Glu[81] is absent in η and γ). Thus, it is expected that dimer formation is stabilized by multiple electrostatic interactions, although the func-

This work was supported in part by Australian National Health and Medical Research Council Project Grant 1068087 (to J. A. C.), National Health and Medical Research Council Program Grant 1071897 (to A. F. L.), and the Fay Fuller Foundation. The authors declare that they have no conflicts of interest with the contents of this article.

This article contains Videos S1–S3.

[1] These authors contributed equally to this work.

[2] To whom correspondence should be addressed. Tel.: 618-8222-3306; Fax: 618-8232-4092; E-mail: Joanna.Woodcock@health.sa.gov.au.

[3] Co-senior authors.

[4] Supported by National Health and Medical Research Council Senior Research Fellowship 1042589.

tional role of these individual salt bridges in dimer stability has not been formally tested.

Distinct from their phosphoserine-binding capabilities, 14-3-3 proteins possess molecular chaperone activity, preventing temperature-induced aggregation of target proteins (8) in a manner similar to that of small heat-shock proteins (sHsps)[5] (9). The molecular mechanism of 14-3-3ζ's chaperone action, however, is poorly understood. We previously showed that neither the phosphoserine-binding groove nor the flexible C-terminal extension is necessary for 14-3-3ζ's chaperone activity (4), implying that the chaperone-competent regions of the protein are distinct from those used for canonical phosphoserine binding. Subsequent studies by Sluchanko *et al.* (10, 11) have shown that a dimer-disrupted mutant of 14-3-3ζ in which residues in the first α-helix are mutated has enhanced chaperone capability, suggesting that exposure of the dimer interface may play a role in 14-3-3ζ's molecular chaperone mechanism.

Previously, we established that phosphorylation of a single serine residue hidden in the dimer interface of 14-3-3ζ (Ser^{58}) disrupted the dimeric structure of the protein (12), and similarly, the phospho-mimic mutations, S58D and S58E, are also dimer-disrupting (13, 14). In this study, we examined 14-3-3ζ mutants lacking the key salt-bridging residues, Asp^{21} and Glu^{89}, in comparison with the S58D phospho-mimic, to determine the relative roles of these residues in stabilizing the dimeric structure of 14-3-3ζ. The mutant proteins were assessed for effects on protein structure, dimer stability, and also molecular chaperone ability. The results provide insight into the dynamics of dimer formation and the molecular basis of chaperone function. Together, the data reveal hitherto unknown features of 14-3-3 protein structure and hint at important aspects of 14-3-3 biology in relation to its chaperone function.

Results

Mutation of putative salt-bridging residues in the 14-3-3ζ dimer interface alters protein structure but does not prevent dimerization

The 14-3-3ζ crystal structure revealed that 620 $Å^2$ is buried at the dimer interface and suggested that salt bridges across this interface hold the monomer subunits together (15). The dimer interface between the 14-3-3ζ subunits comprises two separate faces of interaction that are juxtaposed with 2-fold rotational symmetry (Fig. 1, *A* and *B*). The proposed salt bridges include Arg^{18}-Glu^{89} and Asp^{21}-Lys^{85}, which are conserved across most isoforms (Fig. 1*C*). To determine the role of these putative interactions in dimer stabilization, we carried out conservative substitution of Asp^{21} and Glu^{89} to remove charged residues and disrupt salt-bridge capability. The resulting mutant proteins, D21N and E89Q, were compared with wild-type 14-3-3ζ protein and the phospho-mimic mutant, S58D (an established dimer-disrupting mutant (13)), for their effect on dimer stability using a variety of biochemical and biophysical techniques.

[5] The abbreviations used are: sHsp, small heat-shock protein; CTAB, cetyltrimethylammonium bromide; HDX, hydrogen-deuterium NH exchange; AUC, analytical ultracentrifugation; ADH, alcohol dehydrogenase; SAXS, small-angle X-ray scattering; bis-ANS, 4,4′-dianilino-1,1′-binaphthyl-5,5′-disulfonic acid, dipotassium salt.

Native PAGE and chemical cross-linking analysis have both been employed previously to demonstrate the dimer-destabilizing effect of Ser^{58} phosphorylation (12) and of the phospho-mimic S58D mutation in 14-3-3ζ (13). By native PAGE analysis, the migration of both D21N and E89Q was ostensibly the same as that of wild-type dimeric 14-3-3ζ, whereas S58D exhibited faster migration on the gel, consistent with a more monomeric structure (Fig. 2*A*). Using glutaraldehyde cross-linking, we found that, unlike S58D, D21N and E89Q 14-3-3ζ both formed cross-linked dimers similar to wild type (data not shown). Therefore, the two salt bridge mutants can form dimers, unlike the phospho-mimic mutant, S58D.

Limited trypsinolysis studies have been used previously to determine the effect of phospho-mimic mutants on 14-3-3ζ structure (14). We used the same low-salt and magnesium-free conditions to examine the susceptibility of D21N and E89Q to trypsin and found that both mutant proteins were sensitive to digestion (Fig. 2*B*). Under the same conditions, the wild-type protein was relatively resistant, whereas S58D was also effectively digested, similar to D21N and E89Q (and the related phospho-mimic mutant S58E (14)). Thus, although the salt-bridging mutants, D21N and E89Q, can form dimers, their overall protein structure is more dynamic than the wild-type protein, rendering them susceptible to trypsin digestion.

Analytical ultracentrifugation reveals altered dimer–monomer equilibria of 14-3-3ζ salt bridge mutants

To accurately assess the dimer stability of D21N, E89Q, and S58D mutants relative to wild type, the solution properties of the proteins were analyzed by analytical ultracentrifugation (AUC) (Fig. 3). Initial experiments were undertaken using 0.27 mg/ml 14-3-3ζ protein (9.7 μM monomer) at 20 °C. Sedimentation velocity analysis of wild type 14-3-3ζ detected a predominant species (> 99%) with a standardized sedimentation coefficient of 3.8 S and a very minor secondary species of 6.2 S (Fig. 3*A* and Table 1). The continuous mass ($c(M)$) distribution yielded molecular masses of ~54 and 108 kDa, respectively, for these two species, which correspond closely to the expected masses of dimeric and tetrameric 14-3-3ζ, respectively. A tetrameric form of 14-3-3ζ has not previously been reported in solution, although 14-3-3 crystal structures have been resolved with a tetrameric unit cell (*e.g.* Protein Data Bank entry 2C63, η structure published by Yang *et al.* (16)). By contrast, sedimentation velocity analysis of D21N, E89Q, and S58D 14-3-3ζ mutants at 0.27 mg/ml showed broader sedimentation coefficient distribution profiles with lower standardized sedimentation coefficient values compared with wild-type 14-3-3ζ (Fig. 3*A* and Table 1). This is consistent with a shift in the equilibrium for the mutants toward a less dimeric species and was particularly evident for the known dimer-disrupting phospho-mimic S58D mutant (Fig. 3*A*, *dotted line*). The AUC data indicate that the point mutants D21N and E89Q do promote dimer dissociation, consistent with their predicted role in intermolecular salt bridging of dimers, although they are less dimer-disruptive than the phospho-mimic S58D mutant.

In previous studies with the phospho-mimic mutant S58E, effects on dimer stability were demonstrated to be dependent

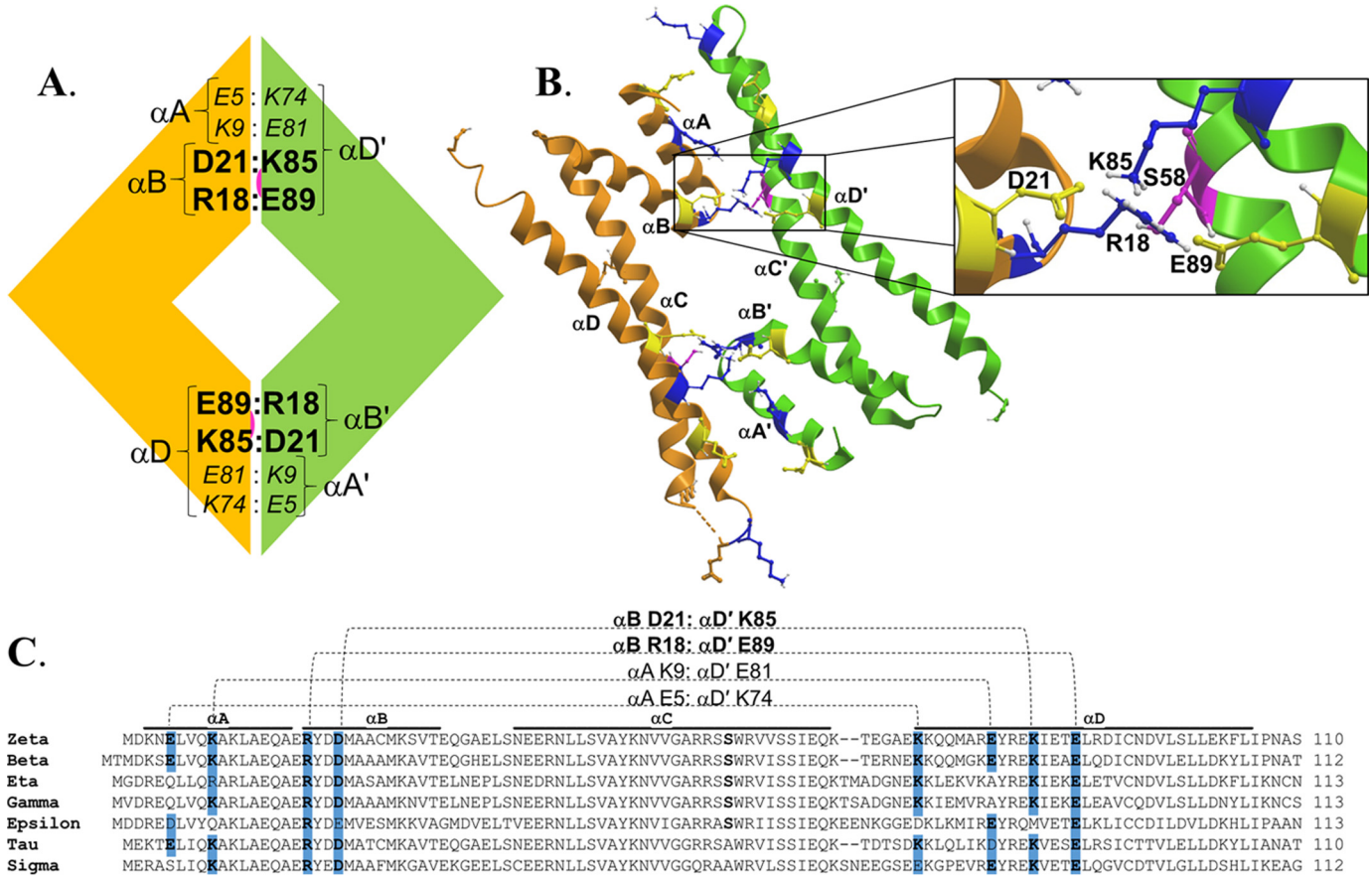

Figure 1. Structural organization of the dimer interface in 14-3-3ζ. *A*, schematic representation of the predicted salt bridges at the dimer interface of 14-3-3ζ. The *orange* and *green modules* represent two monomer units of 14-3-3ζ, and residues shown in *large boldface type* represent predicted salt-bridging residues conserved across multiple 14-3-3 isoforms. The buried Ser[58] phosphorylation site is also shown in *pink*. *B*, the dimer interface of 14-3-3ζ (residues 1–110) is shown in a *ribbon representation* with predicted key salt-bridging residues highlighted (acidic residues in *yellow* and basic residues in *blue*). The buried Ser[58] phosphorylation site is shown in *pink*. The *inset* shows the dimer interface in greater detail with the predicted salt bridge residues *labeled*. *C*, an alignment of the N-terminal primary sequences encompassing the dimer interface of all seven isoforms of human 14-3-3 ζ, β, η, γ, ϵ, τ, and σ, with the predicted salt bridge residues highlighted and their proposed intermolecular interactions represented by *dotted lines*. The positions of the first four α-helices are indicated as *αA*, *αB*, *αC*, and *αD*.

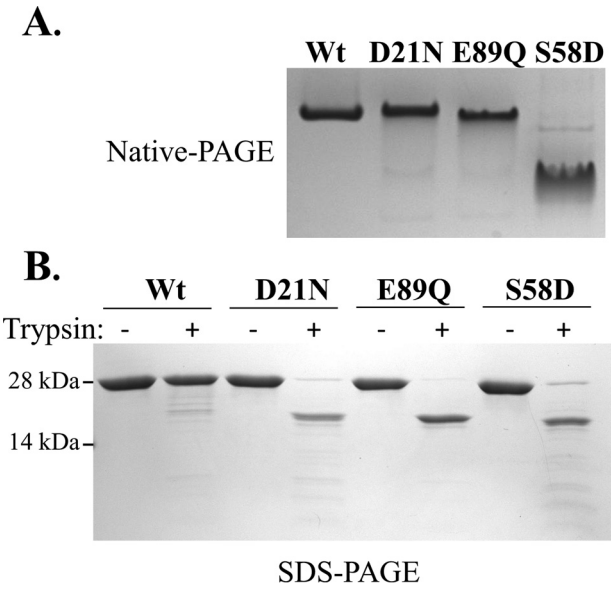

Figure 2. The effect of mutations on 14-3-3ζ protein dimer formation and conformation as demonstrated by native-PAGE analysis (*A*) and limited trypsinolysis (*B*). For trypsinolysis, mutant and wild-type 14-3-3ζ proteins (as *labeled*) were incubated with (+) or without (−) trypsin before separation on SDS-PAGE. Proteins were visualized for *A* and *B* by Coomassie staining.

on protein concentration (14). To investigate the effect of protein concentration on wild-type and mutant 14-3-3ζ dimer dynamics, sedimentation velocity analysis was carried out at a lower protein concentration (Fig. 3*B*). All three 14-3-3ζ mutants exhibited a broadening in sedimentation coefficient distribution profile at the reduced protein concentration (0.09 mg/ml) consistent with further alteration in dimer–monomer dynamics and a decrease in sedimentation coefficient (Fig. 3*B* and Table 1). On close inspection, the D21N sedimentation profile has a detectable shoulder at a lower sedimentation coefficient (~2.2 S), which is also observed at 0.27 mg/ml (Fig. 3*A*, *bottom*) but is more prominent at the lower protein concentration (Fig. 3*B*, *bottom*) and presumably represents monomeric D21N 14-3-3ζ. In comparison, the sedimentation coefficient distribution profile for the wild-type 14-3-3ζ protein at 0.09 mg/ml (Fig. 3*B*) is similar to that at 0.27 mg/ml (Fig. 3*A*), despite a slight decrease in sedimentation coefficient (Table 1), indicating that dimeric wild-type 14-3-3ζ is predominant and stable, even at lower protein concentrations.

Finally, the effect of increased temperature on the dimer–monomer equilibrium for wild-type and mutant 14-3-3ζs was

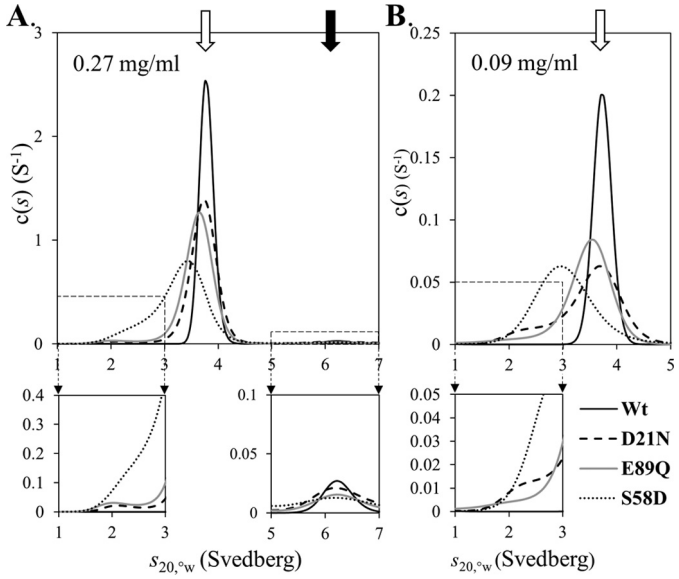

Figure 3. Sedimentation velocity *c*(*s*) profiles of wild-type and mutants of 14-3-3ζ at 0.27 mg/ml (*A*) and 0.09 mg/ml (*B*): 14-3-3ζ wild type (*solid line*), S58D (*dotted line*), D21N (*dashed line*), and E89Q (*gray line*). The position of the 3.75 S dimeric species is indicated by the *open arrow*, and that of the 6.20 S tetrameric species is shown by the *solid black arrow* (in *B* only). The *insets* show expansions of the profiles for the indicated regions. In *A*, root mean square deviation for fit of wild-type 14-3-3ζ is 0.00627, and the values for S58D, D21N, and E89Q are 0.00507, 0.00577, and 0.00544 with run test *z* values of 5.42, 7.15, 14.6, and 11.82 respectively. *B*, root mean square deviation for fit of wild-type 14-3-3ζ is 0.00471, and the values for S58D, D21N, and E89Q are 0.00472, 0.00457, and 0.00485 with run test *z* values of 3.71, 1.12, 0.08, and 1.97, respectively.

Table 1

Sedimentation coefficient of recombinant wild type and mutant 14-3-3ζ proteins

The sedimentation velocity data were fitted to a continuous sedimentation coefficient (*c*(*s*)) distribution model using the program SEDFIT (www.analyticalultracentrifugation.com). (Please note that the JBC is not responsible for the long-term archiving and maintenance of this site or any other third party hosted site.)

	$s^0_{20,w}$		
14-3-3ζ protein	0.27 mg/ml at 20 °C	0.09 mg/ml at 20 °C	0.09 mg/ml at 37 °C
WT	3.75	3.70	3.64
D21N	3.70	3.65	2.84
E89Q	3.60	3.54	3.10
S58D	3.45	2.90	2.91

analyzed by sedimentation velocity analysis. The sedimentation coefficients of 0.09 mg/ml wild-type and mutant 14-3-3ζ at 20 and 37 °C were compared (Table 1). For wild-type 14-3-3ζ, a small decrease in sedimentation coefficient was detected with increasing temperature, implying a minor shift in the dimer–monomer distribution at the higher temperature. The 14-3-3ζ E89Q mutant also showed a small reduction in sedimentation coefficient at 37 °C compared with 20 °C, whereas D21N exhibited a more drastic reduction in sedimentation coefficient at 37 °C, to a value lower than the dimer-disrupted S58D mutant (Table 1). This indicates a dramatic alteration in dimer–monomer dynamics in the D21N mutant protein at the higher temperature, and from all of these results, it appears that the D21N mutation causes a more disruptive effect on 14-3-3ζ dimer–monomer dynamics compared with E89Q, especially at higher temperatures.

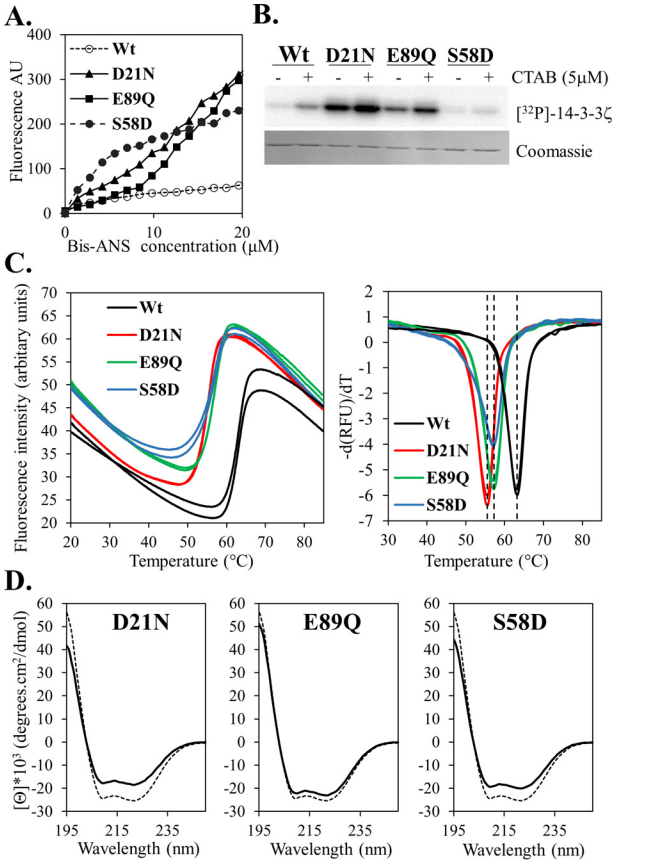

Figure 4. Single amino acid substitutions of 14-3-3ζ cause exposure of the dimer interface and affect protein thermal stability and α-helical organization. *A*, bis-ANS fluorescence profiles for wild-type and mutant 14-3-3ζ proteins. *B*, *in vitro* phosphorylation of wild-type and mutant 14-3-3ζ proteins by PKA in the presence (+) or absence (−) of the sphingomimetic, CTAB. Reactions were separated by SDS-PAGE and analyzed for incorporation of [^{32}P]ATP by autoradiography. The *bottom panel* shows Coomassie staining of the gel. *C*, protein thermal shift analysis of wild-type and mutant 14-3-3ζ proteins using SYPRO-Orange. Representative melt curves are shown in the *left-hand panel*, and first derivatives of those melt curves are shown in the *right-hand* panel. *D*, far-UV CD spectra for the indicated mutants (*solid line*) and wild-type 14-3-3ζ (*dashed line*). All measurements represent the average of three accumulations.

Mutation of Asp^{21} and Glu^{89} in 14-3-3ζ leads to dimer interface exposure

The fluorescent probe bis-ANS is commonly used to assess exposure of hydrophobic regions of proteins whereby bis-ANS fluoresces when bound to exposed clustered hydrophobic regions (17). Previous studies have demonstrated that dimer-disrupted mutants of 14-3-3ζ exhibit enhanced bis-ANS–binding capability, consistent with exposure of hydrophobic regions normally buried in the dimer interface (11, 14). We analyzed the bis-ANS– binding characteristics of S58D 14-3-3ζ protein compared with wild-type 14-3-3ζ at 0.038 mg/ml (1.4 μM monomer) and found that S58D exhibited greater ability to bind bis-ANS compared with wild-type 14-3-3ζ (Fig. 4*A*), indicating greater exposure of hydrophobic surfaces in the dimer-disrupted phospho-mimic mutant. A previous study with bis-ANS binding to the 14-3-3ζ phospho-mimic S58E came to a similar conclusion (14). The salt bridge mutants E89Q and D21N also exhibit increased bis-ANS fluorescence compared with wild-type 14-3-3ζ and distinctive bis-ANS binding char-

Table 2
Secondary structure of recombinant wild-type and mutant 14-3-3ζ proteins
CD data were analyzed using CDPro (sites.bmb.colostate.edu/sreeram/CDPro) with the CONTINLL algorithm (21) and compared with data in the SP43 reference database. (Please note that the JBC is not responsible for the long-term archiving and maintenance of this site or any other third party hosted site.)

14-3-3ζ protein	Composition				
	α-Helix	β-Sheet	Turn	Unordered	Root mean square deviation
	%	%	%	%	%
WT	79.3	0.7	6.1	13.9	0.12
D21N	63.2	5.5	10.6	20.6	0.09
E89Q	74.8	1.7	7.7	15.8	0.11
S58D	67.2	4.1	10.3	18.5	0.08

acteristics compared with S58D (Fig. 4*A*). Whereas S58D exhibited strong bis-ANS fluorescence at low micromolar concentrations (at 5 μM bis-ANS), the D21N and E89Q mutants only exhibited fluorescence at higher bis-ANS concentrations (>5 μM bis-ANS), suggesting a weaker affinity for bis-ANS compared with S58D. Additionally, binding of bis-ANS to D21N and E89Q yielded greater fluorescence than S58D at higher bis-ANS concentrations (>15 μM), suggesting that there are more bis-ANS–binding sites in the salt bridge mutants compared with S58D. These results suggest that the disruptive effects of the salt bridge mutants are quite distinct from the phospho-mimic effects of S58D.

From the original crystal structure of 14-3-3ζ, a number of residues were determined to be buried in the dimer interface, including Ser^{58} in helix αC (15). From our previous studies, Ser^{58} is not accessible for phosphorylation in native wild-type 14-3-3 dimers, and only when the dimer interface is perturbed by sphingosine or a sphingomimetic is a kinase such as PKA or PKC able to phosphorylate Ser^{58} (18, 19). We therefore used Ser^{58} phosphorylation by PKA to assess the accessibility of the dimer interface in the D21N and E89Q mutants. As a control, cetyltrimethylammonium bromide (CTAB) was added, which we showed previously mimics the effect of sphingosine in rendering Ser^{58} accessible for phosphorylation (19). In contrast to wild-type 14-3-3ζ, D21N and E89Q 14-3-3ζ readily underwent phosphorylation even in the absence of the sphingomimetic CTAB (Fig. 4*B*). This was especially noticeable with D21N, which consistently showed a greater degree of phosphorylation in the absence of sphingomimetic compared with E89Q (Fig. 4*B*). S58D did not undergo phosphorylation due to the absence of the Ser^{58} phosphorylation site (Fig. 4*B*). From this, it is concluded that the Ser^{58} phosphorylation site of D21N and E89Q is readily accessible to kinases, indicating that interactions in the dimer interface are weaker in these mutants. Taken together, these analyses demonstrate that mutation of Asp^{21} and Glu^{89} disrupts the dimer interface, leading to exposure of hydrophobic residues with consequent enhanced bis-ANS binding and access to the Ser^{58} phosphorylation site.

Protein thermal shift assays reveal 14-3-3ζ mutant protein instability

The effect of the salt bridge mutations on 14-3-3ζ protein stability relative to wild-type protein was assessed in protein melt analysis using the hydrophobic binding dye SYPRO orange. Multiple melt curves were generated at different protein concentrations for wild-type and mutant 14-3-3ζ proteins but with ostensibly identical results (Fig. 4*C* shows representative results with both temperature melt curves and their first derivatives). The results reveal that the wild type protein has a melt temperature (T_m) of 63 °C compared with 57 °C for E89Q and S58D and 55 °C for D21N. These shifts in T_m indicate reduced protein stability of the mutant 14-3-3ζ proteins relative to wild-type protein, especially with the D21N mutation.

Mutation at Asp^{21} disrupts the α-helical structure of 14-3-3ζ

The effect of the D21N and E89Q mutations on the structural organization of 14-3-3ζ was assessed. The secondary structure of the wild-type and mutant proteins (at 0.19 mg/ml, 6.8 μM monomer) was analyzed by far-UV CD spectroscopy, which produced characteristic spectra with minima at 208 and 222 nm, consistent with the predominantly α-helical structure of 14-3-3ζ (Fig. 4*D*). The residue molar ellipticity at 222 nm of wild-type 14-3-3ζ (the *dashed line* in each *panel* of Fig. 4*D*) agreed well (25,325 degrees cm^2 $dmol^{-1}$) with that reported previously (20). Comparison of the CD spectra of mutant 14-3-3ζ proteins with the wild-type protein indicates that there is some overall change in secondary structure associated with D21N and S58D. Analysis of these CD spectra to assess secondary structure changes using the CONTIN/LL algorithm (21) suggests that there is a marked reduction in α-helical content in both D21N and S58D compared with wild-type 14-3-3ζ (16.1 and 12.1%, respectively; Table 2) with a corresponding increase in β-sheet, turn, and unordered content, whereas E89Q is more similar to wild-type 14-3-3ζ with only a slight reduction in α-helical content (4.5%; Table 2). The 14-3-3ζ phospho-mimic S58E showed a similar loss of α-helicity to S58D (20). Overall, mutation of Asp^{21} caused greater disruption of secondary structure compared with Glu^{89}, suggesting a distinct role for Asp^{21} salt bridges in stabilizing the α-helices at the dimer interface.

The D21N mutant has enhanced chaperone ability toward amorphously aggregating proteins

It has previously been shown that 14-3-3ζ has molecular chaperone activity, inhibiting the amorphous aggregation of proteins under conditions of elevated temperature (8). We demonstrated the chaperone ability of wild type 14-3-3ζ against amorphous aggregation of several target proteins in response to chemical or reduction stress, including insulin, alcohol dehydrogenase (ADH), and α-lactalbumin (4). The chaperone ability of 14-3-3ζ against amorphous aggregation of ADH was previously shown to be enhanced by mutations that disrupt the dimeric structure of 14-3-3, suggesting a role for dimer interface exposure in chaperone function (11). Here, we have

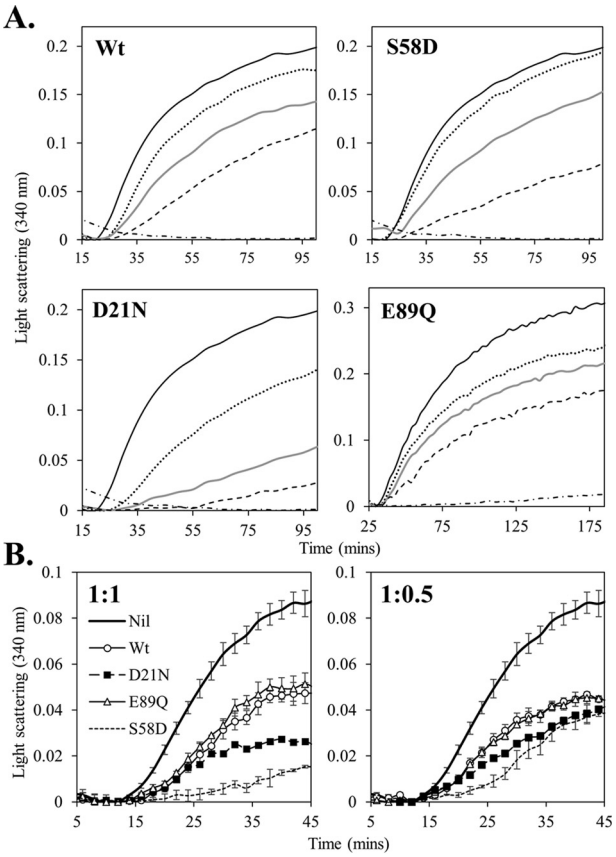

Figure 5. Molecular chaperone activity of wild-type and mutant 14-3-3ζ proteins. *A*, temperature-induced aggregation (at 42 °C) of ADH was monitored by light scattering at 340 nm over time in the absence (*solid line*) and presence of 14-3-3 protein at 1:0.5 (*dotted line*), 1:1 (*gray line*), and 1:2 (*dashed line*) molar ratio of ADH/14-3-3ζ protein. The aggregation of 14-3-3ζ alone is also shown (*dashed and dotted line*). *B*, DTT-induced aggregation of insulin (at 37 °C) was monitored by light scattering at 340 nm over time in the absence (*solid black line*) and presence of 14-3-3 protein at a 1:1 molar ratio (*left-hand panel*) and 1:0.5 molar ratio (*right-hand panel*) of insulin/14-3-3ζ protein. *Error bars*, S.D. of triplicate samples.

assessed the chaperone ability of the D21N, E89Q, and S58D 14-3-3ζ mutants compared with wild-type 14-3-3ζ against the amorphous aggregation of ADH and insulin. Aggregation of ADH was initiated by EDTA chelation of intrinsic Zn^{2+}, which causes unfolding and subsequent aggregation of ADH at 42 °C (4). When the 14-3-3ζ proteins were incubated alone under these conditions, they did not aggregate, allowing ADH aggregation to be monitored by light scattering at 340 nm (Fig. 5*A*). As shown previously, wild-type 14-3-3ζ reduced ADH aggregation in a dose-dependent manner (Fig. 5*A*), reducing ADH aggregation by 40% when present in 2-fold molar excess. The chaperone ability of E89Q 14-3-3ζ was comparable with that of the wild-type protein (Fig. 5*A*), whereas the D21N mutant exhibited enhanced protection against ADH aggregation, reducing aggregation by >80% when in 2-fold molar excess (Fig. 5*A*), indicating greater chaperone activity. S58D also had enhanced chaperone activity relative to wild-type protein (60% reduction in ADH aggregation when in 2-fold molar excess), although not as marked as D21N 14-3-3ζ protein (Fig. 5*A*).

The mutant 14-3-3ζ proteins were also assessed for chaperone activity against DTT-induced insulin B-chain aggregation (Fig. 5*B*). None of the 14-3-3ζ proteins aggregated when incubated with DTT in the absence of insulin (data not shown), allowing insulin aggregation to be monitored by light scattering, similar to ADH. As with ADH aggregation, D21N was a more potent chaperone compared with wild-type and E89Q 14-3-3ζ against insulin aggregation. However, S58D was a more active chaperone than D21N 14-3-3ζ in this system (Fig. 5*B*). It is worth noting that the insulin aggregation assay is incubated at 37 °C, whereas the ADH aggregation assay is at 42 °C, which may account for the relative differences in chaperone activity of D21N 14-3-3ζ protein in the different assays. Our results show that although D21N can form dimers (Fig. 2*A*), the dimers are unstable and readily disrupted by increasing temperature (as shown by AUC (Table 1) and a lower T_m (Fig. 4*C*)). These factors may contribute to D21N's enhanced chaperone activity at higher temperatures.

The D21N 14-3-3ζ mutant exhibits increased hydrogen-deuterium exchange in the N-terminal helices

The CD results with D21N 14-3-3ζ suggest that this mutation causes significant disruption of secondary structure in the N-terminal helices. Hydrogen-deuterium NH exchange (HDX) in combination with mass spectrometry generates information relating to the solvent accessibility, secondary structure (by analyzing hydrogen bonding), and protein conformation and dynamics. HDX has been used previously to examine 14-3-3ζ (7), and therein it was shown that increased deuterium exchange occurred in the N-terminal region of the dimer-disrupted S58D protein compared with wild-type 14-3-3ζ, indicating a more open structural conformation at the dimer interface of the phospho-mimic protein. We have used HDX to compare dynamic changes in dimer-disrupted D21N compared with wild-type protein. We observed a dramatic increase in deuterium exchange in peptides corresponding to the N-terminal region of D21N (amino acids 1–90, encompassing helices αA–αD) compared with wild-type 14-3-3ζ and very little difference in deuterium exchange across all other parts of the proteins (Fig. 6). Four peptides exhibited markedly increased the levels of deuterium exchange in D21N compared with wild-type 14-3-3ζ (labeled *i–iv* in Fig. 6). When the time dependence of deuterium exchange for these four peptides is compared (Fig. 7*A*, *i–iv*), the region exhibiting the most significant increase in deuterium exchange corresponds to the first 22 amino acids, which encompass α-helices A and B and include the Asp^{21} mutation site (Fig. 7*A* (*i*)). This peptide exhibits double the deuterium exchange across the time course in D21N compared with wild-type 14-3-3ζ (Fig. 7*A* (*i*)). Another region corresponding to part of helix αD and encompassing Glu^{89} and the predicted salt-bridging partner of Asp^{21}, Lys^{85}, exhibited a significantly increased rate of deuterium exchange in D21N compared with wild-type protein (Fig. 7*A* (*iv*)). Peptides corresponding to helix αC (Fig. 7*A*, *ii* and *iii*) also exhibited an increased rate of deuterium exchange in D21N compared with wild-type protein and are adjacent to the Ser^{58} phosphorylation site that is readily accessible in D21N but not in the wild-type protein (Fig. 4*B*).

Overlapping peptide sequences were utilized to allow inference of deuterium exchange for individual residues for the D21N mutant compared with wild-type 14-3-3ζ protein at the

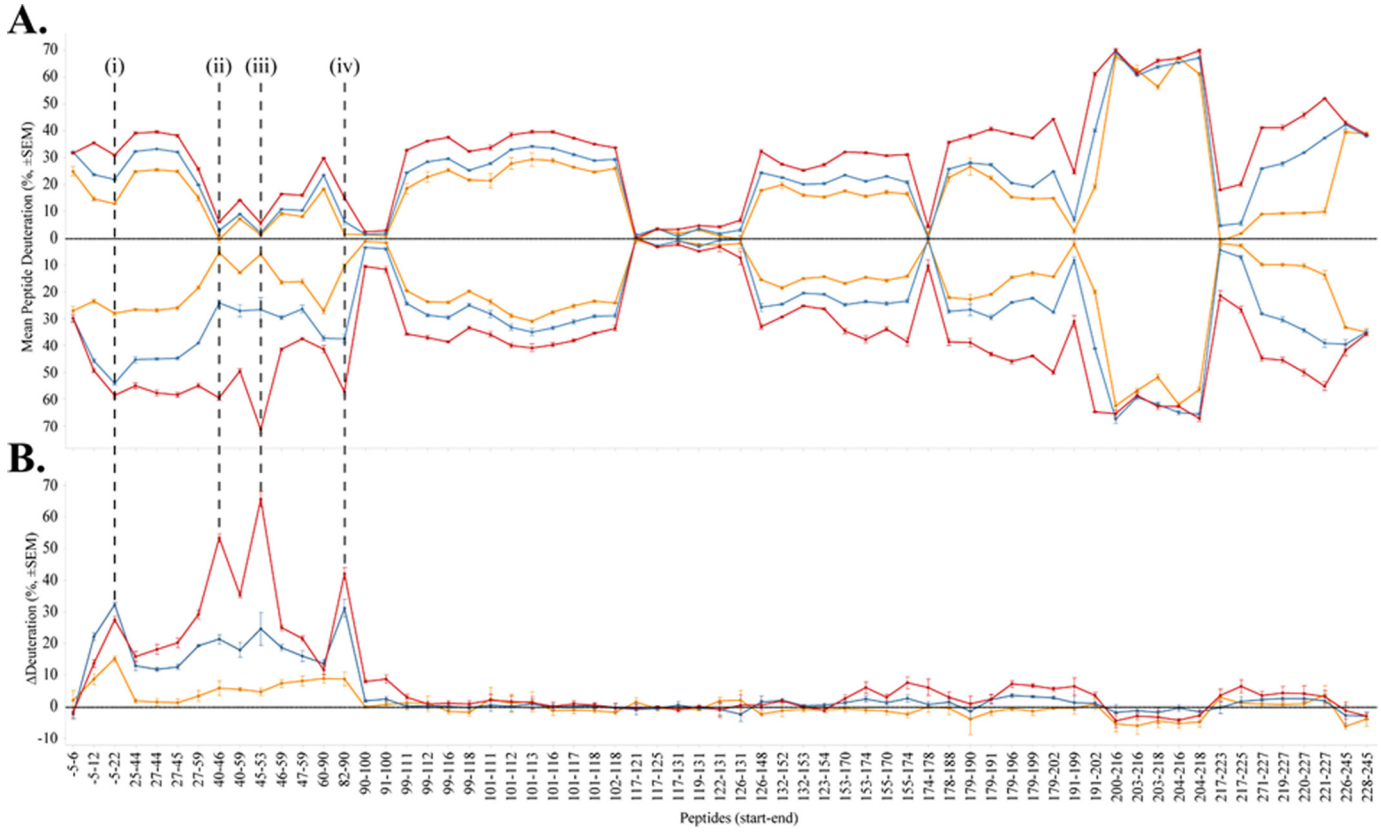

Figure 6. Comparability profiles of HDX of wild-type *versus* D21N 14-3-3ζ. *A*, mirror plot for visual comparison of averaged deuteration of peptides detected from wild-type 14-3-3ζ (*above* the *x* axis) and D21N 14-3-3ζ (*below* the *x* axis). Each point represents a single peptide, and the *orange*, *blue*, and *red lines* represent 1-, 10-, and 60-min time points of HDX, respectively. *Error bars*, S.E. of triplicate determinations. *B*, the difference plot calculated from data in *A* indicates that the main difference in HDX regions is in the N-terminal peptides comprising the first 90 amino acids of the protein, especially peptides from helices αA, αC, and αD of D21N 14-3-3ζ. *i–iv* highlight the peptides showing the greatest difference in HDX between D21N and WT 14-3-3ζ.

three time points used for the HDX study (1, 10, and 60 min). These data were mapped onto the structure of the dimer interface helices (residues 1–110) (Fig. 7*B* and Videos S1–S3). The time-dependent deuterium exchange demonstrated that the focal point for exchange in the dimer interface region was the αA helix–loop–αB helix region (the site of the D21N mutation). HDX in the proximal αC helix of the adjacent monomer and the N-terminal half of the adjoining αD helix was also marked, although slower. This pattern of dimer interface exposure and reduced protein stability is consistent with the altered secondary structure of D21N as determined by CD spectroscopy and also provides a potential mechanism for the altered dimer interface accessibility in the D21N mutant.

Discussion

The functional role of the intermolecular salt bridges in the dimer interface of 14-3-3ζ, although predicted from the crystal structure (15), has not been experimentally tested before. Our results show that the predicted salt-bridging residues, Asp^{21} and Glu^{89}, play important roles in controlling 14-3-3ζ structure and dimer–monomer dynamics. The results also suggest a distinct role for Asp^{21} in maintaining α-helical structural order in the two N-terminal α-helices that make up half of the dimer interface. Conservative charge neutralization of either Asp^{21} or Glu^{89} did not prevent 14-3-3ζ from forming dimers, as determined by native PAGE (Fig. 2*A*) and chemical cross-linking (data not shown), but did alter protein conformation, as detected by limited trypsinolysis (Fig. 2*B*). AUC demonstrated that mutation of either Asp^{21} or Glu^{89} altered the dimer–monomer equilibrium, and the effects were both protein concentration– and temperature–dependent (Fig. 3 and Table 1). Substitution of either Asp^{21} or Glu^{89} exposed hydrophobic regions (as determined by bis-ANS binding; Fig. 4*A*) and also revealed a phosphorylation site (Ser^{58}) otherwise buried in the dimer interface (Fig. 4*B*). Taken together, these results suggest that the salt bridge interactions provided by these residues are key to stabilizing 14-3-3ζ dimer formation. In addition, mutation of Asp^{21} had a greater effect on 14-3-3ζ protein stability than Glu^{89} mutation (as detected using protein melt shift analysis; Fig. 4*C*) and caused significant conformational effects, characterized by a marked loss in α-helical structure (as revealed by CD spectroscopy; Fig. 4*D*) and rapid N-terminal peptide backbone solvent exposure and reduced stability compared with wild-type 14-3-3ζ, especially in the αA helix–loop–αB helix region (as shown by HDX; Figs. 6 and 7). Thus, these studies suggest that Asp^{21} plays an important role in maintaining α-helical integrity at the dimer interface, which probably contributes to dimer dynamics and chaperone activity.

Low-resolution small-angle X-ray scattering (SAXS) of a distinctly monomeric 14-3-3ζ mutant protein has been reported (20) and has revealed a "propensity for disorder" in the N-ter-

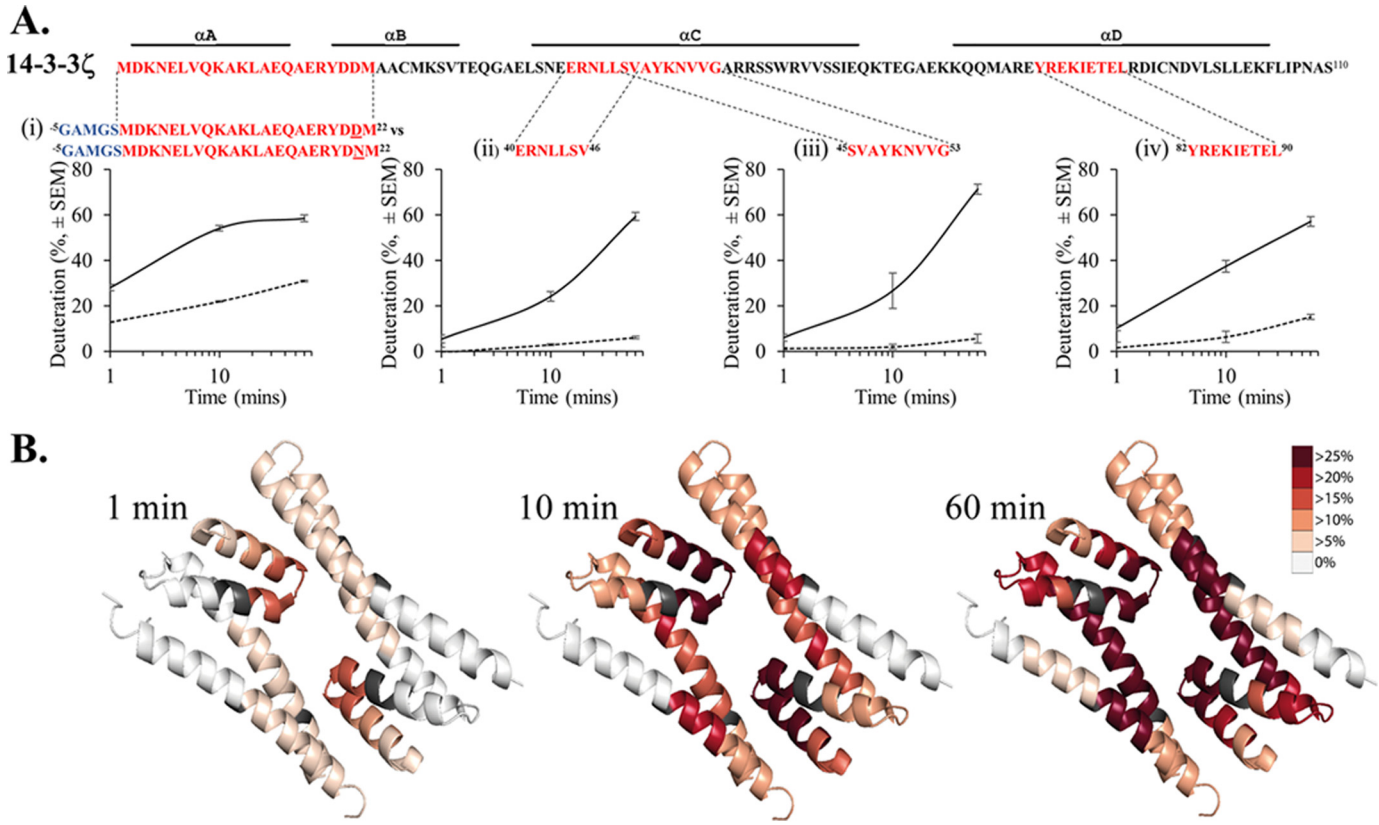

Figure 7. HDX of selected N-terminal peptides of wild-type compared with D21N 14-3-3ζ. *A*, plots show the detail of time-dependent HDX of specific peptides (*i–iv*), as indicated in *red* on the primary sequence (and highlighted in Fig. 6). *Dashed lines* correspond to HDX for wild-type 14-3-3ζ, and *solid lines* are HDX for D21N 14-3-3ζ. The average and S.E. of triplicate determinations are shown. *B*, the *ribbon diagrams* show the comparative HDX of D21N 14-3-3ζ compared with wild-type 14-3-3ζ inferred for individual residues across the dimer interface (residues 1–110) at the three different time points (1, 10, and 60 min) and expressed using *heat map coloring*.

minal helices of the mutant. This contrasts dramatically with the ordered α-helical structure determined by X-ray crystallography of wild-type 14-3-3ζ (15) but may parallel our results with D21N 14-3-3ζ. The monomeric mutant used for the SAXS analysis combined the phospho-mimic mutation, S58E, together with the previously characterized dimer-disrupting ^{12}LAE → ^{12}QQR substitution in helix αA of 14-3-3ζ (22). The combination of these dimer-disrupting mutations produces a profoundly monomeric 14-3-3ζ species, which, interestingly, by CD spectroscopy analysis showed a 12–16% loss of α-helicity compared with the wild-type protein (20), similar to our results with D21N 14-3-3ζ. Furthermore, modeling of the SAXS data from this combination monomeric 14-3-3ζ mutant revealed poor structural resolution of the N-terminal 40 amino acids, indicating that the αA helix–loop–αB helix region is disordered (20). Our results with D21N suggest a similar α-helical disordering effect, which, strikingly, was achieved by conservative substitution of a single amino acid residue and implies that the salt-bridging function of Asp^{21} acts as a gate-keeper for disorder in the dimer interface and may play an important role in dimer dynamics and function.

From previous studies, we know that 14-3-3 dimers are in dynamic exchange, as heterodimers form readily upon mixing of homodimers of different isoforms (16). This indicates that the dimers are in constant equilibrium, although monomeric species of wild-type 14-3-3 proteins are rarely, if at all, detected either *in vitro* or in cells. The question remains, how is monomer subunit exchange achieved? Intermolecular salt bridges must break for subunits to exchange, and thus, the structural changes revealed by D21N substitution may provide clues to how subunit exchange occurs. In wild-type 14-3-3 proteins, the 2-fold rotational symmetry of the dimer interface would allow one half of the dimer interface to remain interactive through salt-bridging while the other half is disengaged. This "breathing" of the dimer interface could provide the plasticity required for regulation of dimer–monomer equilibrium and explain the absence of monomers by standard detection techniques. We can therefore envisage that N-terminally disordered forms of 14-3-3ζ, as illustrated by D21N, may reflect normal changes that occur in the dimer–monomer equilibrium of wild-type 14-3-3ζ.

Our studies on the regulation of 14-3-3 dimers by phosphorylation revealed the role of sphingosine in rendering Ser^{58} in helix αC of dimeric 14-3-3ζ (and analogous residues in other isoforms) accessible to phosphorylation (12). The effect of phosphorylation on Ser^{58} in disrupting the dimeric structure of 14-3-3ζ and other isoforms is well established (12, 18) and mimicked by S58D and S58E mutants of 14-3-3ζ (13, 14). We have also identified new sphingomimetic molecules that can render Ser^{58} phosphorylatable and that, as a consequence of their 14-3-3-targeting effects, exhibit anti-cancer properties (19). It is still unclear, however, how sphingosine and sphingomimetics allow access of kinases to Ser^{58} before the dimer-disrupting effect of phosphorylation. The strong Ser^{58} phosphorylation observed with D21N indicates that Ser^{58} in this

mutant is already exposed, even in the absence of sphingosine or sphingomimetics. Additionally, the HDX analysis also shows that unfurling of the dimer interface in the D21N mutant exposes the αC helix (in the region of Ser^{58}), as well as αA and αB helices (Fig. 7). Thus, if the dimer interface of 14-3-3ζ is in constant flux and N-terminal helices are alternately undergoing "order-to-disorder" transition as the dimer breaths, sphingosine could exert its effect by trapping the protein in the intermediate disordered state and thereby render Ser^{58} accessible.

Compared with the phospho-client binding capability of 14-3-3ζ, the molecular chaperone activity of 14-3-3ζ is poorly understood. In most cases, the dimeric state of 14-3-3 proteins is important for 14-3-3's influence on phospho-clients, whereas previous studies have suggested that monomeric forms of 14-3-3ζ have greater chaperone capacity due, in part, to exposed hydrophobic regions that would otherwise be buried in the dimer interface (23). This hypothesis was supported by the dimer-disrupting helix αA mutant of 14-3-3ζ ^{12}LAE → ^{12}QQR, which had enhanced chaperone activity compared with the wild-type protein (10, 11). Our studies show that the 14-3-3ζ S58D mutant, which is profoundly dimer-disrupted (as shown by native PAGE, cross-linking, and AUC; Figs. 2 and 3 and Table 1) and exhibits exposure of hydrophobic residues compared with wild-type 14-3-3ζ (as shown by enhanced bis-ANS binding; Fig. 4*A*), has greater chaperone activity against heat-induced ADH and DTT-induced insulin aggregation than wild-type protein (Fig. 5). In contrast, the D21N and E89Q 14-3-3ζ mutants are less dimer-disrupting than S58D and are ostensibly dimeric at room temperature (Figs. 2 and 3). Both D21N and E89Q exhibit altered dimer dynamics with increasing temperature, but only D21N exhibits improved chaperone ability relative to wild-type protein and in a temperature-dependent manner. The α-helix–disordering effect of the D21N mutation may provide the key to the enhanced chaperone activity of this mutant. By analogy, N-terminal α-helix disordering in the ^{12}LAE → ^{12}QQR mutant combined with S58E (which was observed by SAXS and CD (20)) may similarly contribute to the enhanced chaperone activity observed previously (10, 11). Similarly, the S58D mutation causes disruption of the α-helical organization of the 14-3-3ζ protein (as detected by CD; Fig. 4*D* and Table 2) and was shown previously (by HDX) to exhibit marked deuterium exchange in the N-terminal α-helices (7), akin to D21N. Thus, not just dimer interface exposure, but also structural disorder in the N-terminal α-helices, may be key to the chaperone function of 14-3-3ζ (20, 24).

sHsps, the major intracellular molecular chaperones involved in preventing protein aggregation, contain large regions of structural disorder in their N- and C-terminal regions (9, 25, 26). There is evidence that order-to-disorder transitions in these regions of sHsps mediate interaction with partially folded aggregating target proteins during chaperone action (27). Similar order-to-disorder changes in the N-terminal helices of 14-3-3ζ may also play a role in the chaperone action of 14-3-3ζ, whereby D21N-like partially disordered and dissociated species represent the chaperone-competent forms of 14-3-3ζ. The chaperone function of sHsps also involves dynamic interchange of subunits. Like the 14-3-3 proteins, sHsps form homo- and heterodimeric as well as oligomeric species that can "hold" partially folded target proteins to prevent their aggregation, with the dissociated dimer species as the probable chaperone-active species (9, 25, 26). The exchange of sHsp subunits is involved in chaperone activity, and by analogy, 14-3-3ζ subunit exchange may also play a role in its chaperone action. Future investigation of 14-3-3ζ in relation to dimer–monomer dynamics may provide clues to the role of 14-3-3 proteins in pathological conditions involving protein aggregation, such as Alzheimer's and Parkinson's diseases.

Experimental procedures

Recombinant 14-3-3 protein production

Recombinant wild-type and mutant proteins were generated as His-tagged fusion proteins expressed from pPROEx-HTb constructs. Mutant 14-3-3ζ constructs (D21N, E89Q, and S58D) were generated using QuikChange site-directed mutagenesis (Qiagen Pty. Ltd., Chadstone Centre, Australia), and mutations were confirmed by DNA sequencing. Wild-type and mutant 14-3-3ζ proteins were produced in the *Escherichia coli* strain, BL21, after isopropyl 1-thio-β-D-galactopyranoside induction, and purified from lysates by affinity chromatography on prepacked nickel-Sepharose columns (GE Healthcare). His-tagged proteins were then cleaved using tobacco etch virus protease.

Native PAGE analysis

Native PAGE was carried out as described previously (12).

Cross-linking of 14-3-3ζ proteins with glutaraldehyde

Wild-type and mutant 14-3-3ζ proteins (250 ng in 10 μl) were incubated with 0.005% (w/v) glutaraldehyde at 37 °C for 15 min before separation on 12.5% (w/v) SDS-PAGE and Western transfer by immunoblotting with K19 14-3-3 antibody (Santa Cruz Biotechnology, Inc., sc-629, lot I1914). Immunoblots were visualized by chemiluminescence on an LAS 4000 biomolecular imager (GE Healthcare).

Limited trypsinolysis

Wild-type and mutant 14-3-3ζ proteins (5 μg at 0.5 mg/ml) were incubated in low-ionic strength buffer (20 mM Tris acetate, pH 7.6, 10 mM NaCl, 0.1 mM EDTA, and 15 mM β-mercaptoethanol) with L-1-tosylamido-2-phenylethyl chloromethyl ketone–treated trypsin (Worthington) at a weight ratio of 14-3-3ζ/trypsin equal to 75:1 and incubated at 37 °C for 20 min before separation on 15% SDS-PAGE and Coomassie staining.

Analytical ultracentrifugation

Prior to analysis by analytical ultracentrifugation, recombinant 14-3-3ζ proteins were run on size exclusion chromatography on a Superdex 200 column (GE Healthcare) and eluted in 20 mM Tris, 150 mM NaCl, pH 7.4, and fractions were collected corresponding to ~54 kDa. Sedimentation velocity analysis was performed using an XL-A analytical ultracentrifuge (Beckman Coulter) with an 8-hole An-50-Ti rotor using methods similar to those reported previously (28). Briefly, double sector centrifuge cells with quartz windows were loaded with 380 μl of protein sample and 400 μl of buffer (20 mM Tris-HCl, 150 mM NaCl, pH 7.4). To determine the optimal wavelength and radial

range for the experiments, initial scans were taken at 3000 rpm. Sedimentation velocity experiments of recombinant 14-3-3ζ wild-type and mutant proteins (3.2 and 9.7 μM monomer) were undertaken at temperatures of 20 and 37 °C and at a rotor speed of 40,000 rpm. Absorbance *versus* radial profiles were obtained using a step size of 0.003 cm at 280 nm every 5 min without averaging. The sedimentation velocity data were fitted to a continuous sedimentation coefficient ($c(s)$) distribution model using the program SEDFIT (www.analyticalultracentrifugation.com).[6] The partial specific volume, buffer density, and viscosity of the 14-3-3ζ proteins were calculated using the program SEDNTERP (29).

Bis-ANS binding analysis

A stock solution of bis-ANS (Invitrogen) was made in 50 mM phosphate buffer, pH 7.4, and 100 mM NaCl. The concentration was determined by UV absorbance at 395 nm, using an extinction coefficient of 23,000 M^{-1} cm^{-1} (30). The 14-3-3ζ proteins at 1.4 μM (0.038 mg/ml of monomer) were titrated with a stock solution of bis-ANS (2.8 mM) over a range of concentrations to give a final concentration of 28 μM (20 molar eq). The fluorescence of each solution at 37 °C was collected via direct excitation at 385 nm (emission collected between 400 and 600 nm) and via FRET excitation at 295 nm (emission collected between 300 and 600 nm) on a Cary eclipse fluorescence spectrophotometer with a Peltier temperature controller (Varian, Melbourne, Australia). The excitation and emission slit widths were set to 5 nm.

Phosphorylation assays

Wild-type and mutant 14-3-3ζ proteins (0.5 μg) in 10 mM Tris-HCl, pH 7.4, were incubated with 5 μM CTAB (Sigma-Aldrich) delivered in 0.3% DMSO for 5 min at room temperature before the addition of 0.25 units of catalytic PKA (Sigma-Aldrich) in kinase reaction buffer (10 mM Tris-HCl, pH 7.4, 15 mM $MgCl_2$, 0.3 mM DTT, 25 μM ATP, and 0.3 μCi of [^{32}P]ATP). Samples were incubated at 37 °C for 20 min and then separated on 12.5% (w/v) SDS-PAGE. The phosphorylated 14-3-3ζ was detected using a Typhoon PhosphorImager.

Protein thermal shift assays

Wild-type and mutant 14-3-3ζ proteins at 1.3 mg/ml in 50 mM phosphate, pH 7.4, 100 mM NaCl were incubated in 20 μl with 10× SYPRO-Orange (Sigma-Aldrich) in a sealed 384-well white plate on a Roche Applied Science Lightcycler 480, and fluorescence was measured over a temperature ramp of 20–85 °C following manufacturer's instructions.

CD spectroscopy

The far-UV CD spectra of the 14-3-3ζ proteins at 7.2 μM (0.19 mg/ml) were recorded on a Jasco J-815 spectropolarimeter (ATA Scientific) over a wavelength range of 195–250 nm with a scan rate of 50 nm/min and a bandwidth of 1 nm. All measurements were obtained at 20 °C in 20 mM phosphate buffer, pH 7.4, and represent the average of three accumulations. All high-voltage tension readings above 600 V were discarded, and the data were converted to mean residue ellipticity. Data were analyzed using the CONTINLL algorithm and SP43 database from the CDPro software package (sites.bmb.colostate.edu/sreeram/CDPro)[6] (21).

Chaperone assays

Amorphous aggregation assays were undertaken in triplicate in 50 mM phosphate buffer, 100 mM sodium chloride, and 2 mM EDTA, pH 7.4, in clear 96-well plates (Greiner Bio-One, Baden-Wurttemberg, Germany) and monitored by light scattering at 340 nm using a Fluostar Optima plate reader (BMG Labtechnologies, Mornington, Australia). ADH (14 μM; Sigma-Aldrich) was incubated in the absence or presence of 14-3-3ζ proteins at a 1:0–2 molar ratio of ADH to 14-3-3ζ monomers, and assays were incubated at 42 °C to induce amorphous aggregation. Insulin (Sigma-Aldrich) at 44 μM was incubated in the absence or presence of 14-3-3ζ proteins at a 1:0–1 molar ratio of insulin to 14-3-3ζ monomers, and aggregation monitored after the addition of 1 mM DTT at 37 °C.

HDX

Experiments were initiated by 20-fold dilution of 14-3-3ζ protein (2.8 μg, 100 pmol) in deuterated buffer containing 10 mM Tris-HCl, pD 7.5. Aliquots were taken at several time points (1, 10, and 60 min) with the HDX reaction suppressed by acidification of the sample to pH 2.5 using formic acid before snap-freezing in liquid nitrogen. Digestion of the protein was carried out by thawing the sample in a 10-fold dilution of H_2O before the addition of an equimolar concentration of pepsin (Sigma-Aldrich) for 2 min on ice. Peptides were subjected to LC-MS analysis using an 1100 series high-performance liquid chromatograph (Agilent) coupled to an LTQ-Orbitrap XL (Thermo). Peptides were loaded onto an in-house packed, reverse-phase trap column (ReproSil-Pur C18 (Dr. Maisch GmbH, Ammerbuch, Germany); 2 × 2 mm, 5 μm) before separation on an in-house packed, reverse-phase analytical column (ReproSil-Pur C18 (Dr. Maisch GmbH); 200 μm × 150 mm, 3 μm). Peptides were loaded onto the column at 5% acetonitrile, 0.2% formic acid, and elution was performed using a gradient rising from 5 to 50% acetonitrile over 6 min and then 85% acetonitrile for 1 min before reconditioning the column at 5% acetonitrile for 5 min. Spectra were acquired in positive ion mode with m/z range from 350 to 1850. Deuteration of peptides was determined by analysis of samples using HDX Workbench as described previously (31).

[6] Please note that the JBC is not responsible for the long-term archiving and maintenance of this site or any other third party hosted site.

Author contributions—J. M. W. coordinated the studies and performed and analyzed some experiments. K. L. G. conducted many of the experiments and analyzed the results, which formed the basis of her Ph.D. thesis (32). J. J. S. performed and analyzed the HDX studies with intellectual input from A. I. W. C. C. provided technical assistance and contributed to Figs. 2 and 4. M. A. P. provided AUC expertise and helped analyze and interpret the AUC results in Fig. 3. S. M. P., A. F. L., and J. A. C. provided intellectual input and together with J. M. W. contributed to interpretation of the data and writing the paper. All authors reviewed the results and approved the final version of the manuscript.

Acknowledgments—We acknowledge the La Trobe University-Comprehensive Proteomics Platform for access to analytical ultracentrifugation instrumentation and the Biophysical Characterization Facility at the University of South Australia for access to the CD spectropolarimeter. This work was made possible through Victorian State Government Operational Infrastructure Support, the L. E. W. Carty Charitable Fund, and the Ian Rollo Currie Estate Foundation for infrastructure support.

References

1. Gardino, A. K., and Yaffe, M. B. (2011) 14-3-3 proteins as signaling integration points for cell cycle control and apoptosis. *Semin. Cell Dev. Biol.* **22,** 688–695 CrossRef Medline
2. Morrison, D. (2009) The 14-3-3 proteins: integrators of diverse signalling cues that impact cell fate and cancer development. *Trends Cell Biol.* **19,** 16–23 CrossRef Medline
3. Kaneko, K., and Hachiya, N. S. (2006) The alternative role of 14-3-3 zeta as a sweeper of misfolded proteins in disease conditions. *Med. Hypotheses* **67,** 169–171 CrossRef Medline
4. Williams, D. M., Ecroyd, H., Goodwin, K. L., Dai, H., Fu, H., Woodcock, J. M., Zhang, L., and Carver, J. A. (2011) NMR spectroscopy of 14-3-3ζ reveals a flexible C-terminal extension: differentiation of the chaperone and phosphoserine-binding activities of 14-3-3ζ. *Biochem. J.* **437,** 493–503 CrossRef Medline
5. Gardino, A. K., Smerdon, S. J., and Yaffe, M. B. (2006) Structural determinants of 14-3-3 binding specificites and regulation of subcellular localization of 14-3-3-ligand complexes: a comparison of the X-ray crystal structures of all human 14-3-3 isoforms. *Semin. Cancer Biol.* **16,** 173–182 CrossRef Medline
6. Obsilova, V., Herman, P., Vecer, J., Sulc, M., Teisinger, J., and Obsil, T. (2004) 14-3-3ζ C-terminal stretch changes its conformation upon ligand binding and phosphorylation at Thr^{232}. *J. Biol. Chem.* **279,** 4531–4540 CrossRef Medline
7. Haladová, K., Mrázek, H., Ječmen, T., Halada, P., Man, P., Novák, P., Chmelík, J., Obšil, T., and Šulc, M. (2012) The combination of hydrogen/deuterium exchange or chemical cross-linking techniques with mass spectrometry: mapping of human 14-3-3ζ homodimer interface. *J. Struct. Biol.* **179,** 10–17 CrossRef Medline
8. Yano, M., Nakamuta, S., Wu, X., Okumura, Y., and Kido, H. (2006) A novel function of 14-3-3 protein: 14-3-3ζ is a heat-shock-related molecular chaperone that dissolves thermal-aggregated proteins. *Mol. Biol. Cell* **17,** 4769–4779 CrossRef Medline
9. Treweek, T. M., Meehan, S., Ecroyd, H., and Carver, J. A. (2015) Small heat-shock proteins: important players in regulating cellular proteostasis. *Cell Mol. Life Sci.* **72,** 429–451 CrossRef Medline
10. Sluchanko, N. N., Artemova, N. V., Sudnitsyna, M. V., Safenkova, I. V., Antson, A. A., Levitsky, D. I., and Gusev, N. B. (2012) Monomeric 14-3-3ζ has a chaperone-like activity and is stabilized by phosphorylated HspB6. *Biochemistry* **51,** 6127–6138 CrossRef Medline
11. Sluchanko, N. N., Roman, S. G., Chebotareva, N. A., and Gusev, N. B. (2014) Chaperone-like activity of monomeric human 14-3-3ζ on different protein substrates. *Arch. Biochem. Biophys.* **549,** 32–39 CrossRef Medline
12. Woodcock, J. M., Murphy, J., Stomski, F. C., Berndt, M. C., and Lopez, A. F. (2003) The dimeric *versus* monomeric status of 14-3-3ζ is controlled by phosphorylation of Ser^{58} at the dimer interface. *J. Biol. Chem.* **278,** 36323–36327 CrossRef Medline
13. Powell, D. W., Rane, M. J., Joughin, B. A., Kalmukova, R., Hong, J.-H., Tidor, B., Dean, W. L., Pierce, W. M., Klein, J. B., Yaffe, M. B., and McLeish, K. R. (2003) Proteomic identification of 14-3-3ζ as a mitogen-activated protein kinase-activated protein kinase 2 substrate: role in dimer formation and ligand binding. *Mol. Cell Biol.* **23,** 5376–5387 CrossRef Medline
14. Sluchanko, N. N., Chernik, I. S., Seit-Nebi, A. S., Pivovarova, A. V., Levitsky, D. I., and Gusev, N. B. (2008) Effect of mutations mimicking phosphorylation on the structure and properties of human 14-3-3ζ. *Arch. Biochem. Biophys.* **477,** 305–312 CrossRef Medline
15. Liu, D., Bienkowska, J., Petosa, C., Collier, R. J., Fu, H., and Liddington, R. (1995) Crystal structure of the zeta isoform of the 14-3-3 protein. *Nature* **376,** 191–194 CrossRef Medline
16. Yang, X., Lee, W. H., Sobott, F., Papagrigoriou, E., Robinson, C. V., Grossmann, J. G., Sundström, M., Doyle, D. A., and Elkins, J. M. (2006) Structural basis for protein-protein interactions in the 14-3-3 protein family. *Proc. Natl. Acad. Sci. U.S.A.* **103,** 17237–17242 CrossRef Medline
17. Hawe, A., Sutter, M., and Jiskoot, W. (2008) Extrinsic fluorescent dyes as tools for protein characterization. *Pharm. Res.* **25,** 1487–1499 CrossRef Medline
18. Woodcock, J. M., Ma, Y., Coolen, C., Pham, D., Jones, C., Lopez, A. F., and Pitson, S. M. (2010) Sphingosine and FTY720 directly bind pro-survival 14-3-3 proteins to regulate their function. *Cell Signal.* **22,** 1291–1299 CrossRef Medline
19. Woodcock, J. M., Coolen, C., Goodwin, K. L., Baek, D. J., Bittman, R., Samuel, M. S., Pitson, S. M., and Lopez, A. F. (2015) Destabilisation of dimeric 14-3-3 proteins as a novel approach to anti-cancer therapeutics. *Oncotarget* **6,** 14522–14536 CrossRef Medline
20. Sluchanko, N. N., and Uversky, V. N. (2015) Hidden disorder propensity of the N-terminal segment of universal adapter protein 14-3-3 is manifested in its monomeric form: novel insights into protein dimerization and multifunctionality. *Biochim. Biophys. Acta* **1854,** 492–504 CrossRef Medline
21. Sreerama, N., and Woody, R. W. (2000) Estimation of protein secondary structure from circular dichroism spectra: comparison of CONTIN, SELCON, and CDSSTR methods with an expanded reference set. *Anal. Biochem.* **287,** 252–260 CrossRef Medline
22. Sluchanko, N. N., Sudnitsyna, M. V., Seit-Nebi, A. S., Antson, A. A., and Gusev, N. B. (2011) Properties of the monomeric form of human 14-3-3ζ protein and its interaction with Tau and HspB6. *Biochemistry* **50,** 9797–9808 CrossRef Medline
23. Sluchanko, N. N., and Gusev, N. B. (2012) Oligomeric structure of 14-3-3 protein: what do we know about monomers? *FEBS Lett.* **586,** 4249–4256 CrossRef Medline
24. Sluchanko, N. N., and Gusev, N. B. (2017) Moonlighting chaperone-like activity of the universal regulatory 14-3-3 proteins. *FEBS J.* **284,** 1279–1295 CrossRef Medline
25. Cox, D., Carver, J. A., and Ecroyd, H. (2014) Preventing α-synuclein aggregation: the role of the small heat-shock molecular chaperone proteins. *Biochim. Biophys. Acta* **1842,** 1830–1843 CrossRef Medline
26. Ecroyd, H., and Carver, J. A. (2009) Crystallin proteins and amyloid fibrils. *Cell Mol. Life Sci.* **66,** 62–81 CrossRef Medline
27. Peschek, J., Braun, N., Rohrberg, J., Back, K. C., Kriehuber, T., Kastenmüller, A., Weinkauf, S., and Buchner, J. (2013) Regulated structural transitions unleash the chaperone activity of αB-crytallin. *Proc. Natl. Acad. Sci. U.S.A.* **110,** E3780–E3789 CrossRef Medline
28. Peverelli, M. G., Soares da Costa, T. P., Kirby, N., and Perugini, M. A. (2016) Dimerization of bacterial diaminopimelate decarboxylase is essential for catalysis. *J. Biol. Chem.* **291,** 9785–9795 CrossRef Medline
29. Laue, T. M., and Stafford, W. F., 3rd (1999) Modern applications of analytical ultracentrifugation. *Annu. Rev. Biophys. Biomol. Struct.* **28,** 75–100 CrossRef Medline
30. Sheluho, D., and Ackerman, S. H. (2001) An accessible hydrophobic surface is a key element of the molecular chaperone action of Atp11p. *J. Biol. Chem.* **276,** 39945–39949 CrossRef Medline
31. Pascal, B. D., Willis, S., Lauer, J. L., Landgraf, R. R., West, G. M., Marciano, D., Novick, S., Goswami, D., Chalmers, M. J., and Griffin, P. R. (2012) HDX workbench: software for the analysis of H/D exchange MS data. *J. Am. Soc. Mass Spectrom.* **23,** 1512–1521 CrossRef Medline
32. Goodwin, K. L. (2015) *Localisation of the molecular chaperone site of 14-3-3ζ: an intracellular protein associated with toxic neurological protein aggregates*, Ph.D. thesis, School of Physical Sciences, University of Adelaide